HHS Public Access

Author manuscript

Stroke. Author manuscript; available in PMC 2019 July 01.

Published in final edited form as:

Stroke. 2018 July ; 49(7): 1719–1726. doi:10.1161/STROKEAHA.117.020461.

The diverse inflammatory response after cerebral microbleeds includes coordinated microglial migration and proliferation

Sung Ji Ahn, PhD[1], **Josef Anrather, DVM**[2], **Nozomi Nishimura, PhD**[1], and **Chris B. Schaffer, PhD**[*,1]

[1]Meinig School of Biomedical Engineering, Cornell University, Ithaca NY 14853

[2]Feil Family Brain and Mind Institute, Weill Cornell Medical College, New York NY 10065

Abstract

Background and Purpose—Cerebral microbleeds are linked to cognitive decline, but it remains unclear how they impair neuronal function. Infarction is not typically observed near microbleeds, suggesting more subtle mechanisms, such as inflammation, may play a role. Due to their small size and largely asymptomatic nature, real-time detection and study of spontaneous cerebral microbleeds in humans and animal models is difficult.

Methods—We used in vivo two-photon microscopy through a chronic cranial window in adult mice to follow the inflammatory response after a cortical microhemorrhage of ~100-μm diameter, induced by rupturing a targeted cortical arteriole with a laser.

Results—The inflammatory response included the invasion of blood borne leukocytes, the migration and proliferation of brain resident microglia, and the activation of astrocytes. Nearly all inflammatory cells responding to the microhemorrhage were brain-resident microglia, but a small number of $CX3CR1^{+}$ and $CCR2^{+}$ macrophages, ultimately originating from the invasion of blood-borne monocytes, were also found near the lesion. We found a coordinated pattern of microglia migration and proliferation, where microglia within 200 μm of the microhemorrhage migrated toward the lesion over hours to days. In contrast, microglia proliferation was not observed until ~40 hours after the lesion and occurred primarily in a shell-shaped region where the migration of microglia decreased their local density. This data suggests that local microglia density changes may trigger proliferation. Astrocytes activated in a similar region as microglia, but delayed by a few days. By two weeks, this inflammatory response had largely resolved.

Conclusions—While microhemorrhages are small in size, the brain responds to a single bleed with an inflammatory response that involves brain-resident and blood-derived cells, persists for weeks, and may impact the adjacent brain microenvironment.

Keywords

cerebral microhemorrhages; animal models; nonlinear microscopy; laser ablation

[*]Corresponding Author: Chris B Schaffer, B57 Weill Hall, 526 Campus Road, Cornell University, Ithaca NY 14853, (607)-342-7737, cs385@cornell.edu.

Competing Financial Interests: The authors declare no competing financial interests.

Introduction

Cerebral microbleeds (CMBs) are a manifestation of cerebral small vessel disease and are currently a major topic in clinical cerebrovascular research[1]. CMBs vary in size from tens of micrometers to several millimeters, and occur at increasing frequency with age[2], hypertension[3], cerebral amyloid angiopathy (CAA)[4], anticoagulant treatment[5], and with genetic conditions such as CADASIL[1, 6]. While typically thought of as acutely asymptomatic, several case reports document CMBs leading to transient neurological episodes that include symptoms such as paresthesia, weakness and dysphasia in patients with CAA (where this is termed "amyloid spells")[7] or with CADASIL[6]. Several large studies have linked increased incidence of CMBs to accelerated cognitive decline and to increased risk for dementia[1, 8, 9]. The cellular mechanisms by which CMBs affect the health and function of cells in the brain microenvironment, however, remains poorly understood.

In recent work, we have used a laser-based approach to induce CMBs in the cortex of rodents[10] to explore the impact of these lesions on neurons and surrounding cells. We found that microhemorrhages do not lead to nearby cell death or degeneration of dendritic arbors[11], or to long-term loss of neural responsivity[12]. We did observe an increase in the density of inflammatory cells near the lesion, although the classes of cells involved and their origin was not determined[11]. Consistent with this, the few post-mortem studies of CMBs in the literature tend to report increased presence of inflammatory cells rather than significant tissue infarction[13-15]. Here, we used a laser-induced microhemorrhage model and two-photon excited fluorescence (2PEF) imaging to examine the inflammatory response after a microhemorrhage, identifying some of the cell types involved, their spatiotemporal dynamics, and the mechanisms leading to increased inflammatory cell density near the lesion.

Methods Summary

The data that support the findings of this study are available from the corresponding author upon reasonable request. All animal experiments were conducted in strict accordance with the recommendations in the Guide for the Care and Use of Laboratory Animals published by National Institutes of Health, and all animal procedures were approved by the Cornell University Institutional Animal Care and Use Committee (protocol numbers 2009-0043 and 2015-0029). Detailed Materials and Methods are provided in the Supplementary Information.

To study the inflammatory response to a brain microhemorrhage, we implanted a chronic, glass-covered cranial window over the cortex of adult mice. To distinguish the response of different classes of inflammatory cells to a CMB, we used transgenic fluorescent reporter mouse lines and bone marrow transplant (BMT) chimeras to label different classes of inflammatory cells. After three weeks of recovery, we used a laser-based approach to rupture targeted penetrating arterioles, vessels that branch from the surface arteriole network and dive into the brain to feed capillary beds[12]. We irradiated the edge of the vessel lumen with short bursts of tightly-focused femtosecond laser pulses with sufficient energy to cause ionization of the material at the laser focus. When targeting ~20-μm diameter penetrating

arterioles, a ~100-μm diameter CMB was reliably produced in the cortex[10-12] (Fig. 1, Supplementary Movie), comparable to the size of the smaller bleeds found in post-mortem human brain[16]. This laser irradiation deposited relatively little total energy, so there was minimal collateral damage to surrounding tissue from the laser itself. The ruptured wall of the targeted vessel clotted within a few seconds and restricted the size of the hematoma[11]. Blood flow in the targeted penetrating was not disrupted, so there is no ischemic injury in this model[10]. This approach allows us to control the time and location of a CMB in the cortex, allowing the use of *in vivo* 2PEF microscopy to follow the cellular response to the injury. We followed the invasion, migration, and proliferation of various classes of inflammatory cells at the lesion site over hours to weeks using 2PEF imaging. We also quantified microglia proliferation and confirmed distance and time dependent cell density changes after the lesion using histological approaches in animals that were sacrificed at different time points after inducing a microhemorrhage. Finally, we developed phenomenological computational models of the microglia response to the microhemorrhage based on the migration and proliferation rates we observed.

Results

We first characterized the response of blood-borne monocytes that tend to invade tissue after injury. It has been reported that in animal models of ischemic and hemorrhagic stroke, monocyte-derived tissue macrophages (Mo/MΦ) are among the most numerous blood borne immune cells infiltrating the brain lesion[17, 18]. Previous work has suggested there are two broad classes of these circulating monocytes, inflammatory monocytes, which express CCR2 and exhibit phagocytic, proteolytic, and inflammatory functions, and patrolling monocytes, which express CX3CR1 and tend to attenuate inflammation and participate in wound healing[19]. In wild-type mice receiving bone marrow from *Cx3cr1*$^{GFP/+}$ mice (*Cx3cr1*$^{GFP/+}$ → wild-type mice), primarily patrolling monocytes were labeled. We observed a small number of GFP positive cells (CX3CR1^{+} Mo/MΦ) in the brain tissue near the microhemorrhage beginning a few days to weeks after the lesion (Fig. 2A, top panel), which were nearly all in perivascular locations adjacent to the vessel wall (Fig. 2B, right panel). In mice with inflammatory monocytes labeled with RFP (*Ccr2*$^{RFP/+}$), we observed the presence of a few labeled cells (CCR2^{+} Mo/MΦ) near the injury beginning one to two days after the lesion (Fig. 2A, middle panel), divided about equally between parenchymal and perivascular locations (Fig. 2B). Finally, we imaged mice with all leukocytes labeled (UBC-GFP → wild-type), and, again observed the presence a small number of labeled cells in the brain tissue near the microhemorrhage (Fig. 2A, bottom panel), divided about equally between parenchymal and perivascular locations (Fig. 2B). Small, punctate, autofluorescent spots also appeared over a few days after the lesion. Taken together, these data suggest that a modest number of blood-borne cells appear after a CMB, with more inflammatory CCR2^{+} Mo/MΦ cells present earlier and more CX3CR1^{+} Mo/MΦ cells present later. While there were only a few such blood-derived inflammatory cells present after the microhemorrhage, the time course of the appearance of CCR2^{+} and CX3CR1^{+} cells was similar to that seen after larger ischemic lesions, where blood-borne cells play a larger role[20].

We next determined the role of brain-resident microglia, cells that are known to surveil adjacent tissue by constantly extending and retracting processes[21], and to respond to local

injuries[22]. Without an injury, we saw no significant change in microglia location over weeks (imaged in *Cx3cr1*$^{GFP/+}$ mice), although the spatial pattern made by their processes changed significantly, consistent with surveillance behavior[21] (Supplementary fig. IA). However, in the presence of a microhemorrhage, microglia extended processes toward the microhemorrhage within minutes (Supplementary fig. IB). In *Cx3cr1*$^{GFP/+}$ mice receiving BMT from wild-type mice (wild-type → *Cx3cr1*$^{GFP/+}$) microglia were GFP labeled (as well as a reduced fraction of patrolling monocytes due to incomplete chimerism). The density of GFP-labeled cells within 100 μm of bleed increased over the first two days (Fig. 2C and D). There was a trend toward decreased density of labeled cells at distances of 100-200 μm away from the injury at 1 day, which recovered by two days (Fig. 2D).

We next evaluated the relative role of migration and proliferation in the microglia density increase near the microhemorrhage. We followed the movement of individual microglia over 48 hr after the lesion in *Cx3cr1*$^{GFP/+}$ mice (Fig. 3A and B). Microglia migrated radially inward toward the lesion, with some cells traveling distances of up to 40 μm (Fig. 3C). Microglia initially within 100 μm of the target vessel began to migrate within hours, while cells starting further from the lesion took progressively longer to begin migrating (Fig. 3D). Migration speeds ranged from 0.5 – 2 μm/hour. In microglia that migrated, we observed a stereotypical temporal sequence where the cell first extended processes toward the lesion, then these processes became thicker, and finally the cell body migrated along the path of the thickened process toward the lesion, catching up to the process that was previously extended (Supplementary fig. IB). We also observed proliferation of some microglia using time-lapse 2PEF imaging at times 40 hours or later after the injury, as evidenced by the presence of two microglia at the location of a single, larger microglia from the previous time point (Fig. 4A, Supplementary fig. II). To quantify the role of proliferation in the microglia density increase, we used 5-ethynyl-2′-deoxyuridine (EdU) labeling and immunohistology approaches (Fig. 4B, Supplementary fig. III). Interestingly, we found microglia proliferated predominantly in a ~100-μm wide shell with a ~175-μm radius that surrounded the targeted penetrating arteriole (Fig. 4C and D). Taken together, these data suggest that microglia near a microhemorrhage respond by rapidly migrating toward the injury, leading to a slight decrease in density in the surrounding neighborhood. After ~40 hours, microglia then proliferate in this region where the density had decreased. This pattern of migration and proliferation leads to increased density near the lesion while preserving microglia density farther away. After two days, the microglia density close to the injury began to slowly decline and neared baseline density by 2 weeks, with microglia regaining a more ramified morphology.

The spatial overlap between the regions of microglia density decrease and of microglia proliferation suggests that microglia may be triggered to proliferate when their local density decreases. To explore this idea, we computationally simulated the response of microglia to a microhemorrhage based on the migration rates of microglia measured by *in vivo* imaging (data from Fig. 3, *Cx3cr1*$^{GFP/+}$) and the proliferation probabilities that were assessed histologically (data from Fig. 4D, *Cx3cr1*$^{GFP/+}$) to determine if we could account for the microglia density changes near the lesion. First, we used our experimental measurements to extract probability distributions for microglia migration distances (Supplementary figs. IV and V) and microglia proliferation (Fig. 4D), each as a function of distance from and time

after the microhemorrhage. The resulting simulations showed an increase in microglia density near the lesion over 48 hr that agreed well with the spatially-dependent microglia density measured in separate experiments (data from Fig. 2C and D, wild-type → *Cx3cr1*$^{GFP/+}$), validating this simulation approach (Fig. 5B). A surrounding shell-shaped region with a slightly decreased microglia density at 24 hr was also evident in the simulations and filled in due to proliferation by 48 hr (Fig. 5A and B). To evaluate whether the spatial pattern of microglia proliferation could be recreated based on changes in the local microglia density, we next ran the simulation using experimentally-measured microglia migration distributions but now assuming that microglia were triggered to proliferate if their domain volume increased by more than a defined factor (Fig. 5C and Supplementary fig. VI). We found that the simulation predicted the observed spatial distribution of microglia proliferation using a 50% volume increase as the threshold value to trigger a proliferative event (Fig. 5D).

We also sought to understand the participation of astrocytes in the inflammatory response following a CMB. Although the representation of astrocyte reactivity by the expression level of glial fibrillary acidic protein (GFAP) is still debatable, this approach is widely used. After creating laser-induced microhemorrhages in *Cx3cr1*$^{GFP/+}$ mice, we sacrificed mice at different time points, immuno-stained for GFAP, and imaged GFAP expression as well as GFP-labeled microglia. We saw extensive expression of GFAP around the lesion starting at two days and peaking at seven days after the injury (Fig. 6A). Over time, GFAP expression declined and we did not observe the formation of an astrocytic glial scar near the lesion at later time points (Fig. 6B). Consistent with our *in vivo* imaging, GFP labeling density was highest at two days after the injury and declined afterward, indicating that the peak response of astrocytes was delayed relative to that of microglia.

Discussion

The presence of CMBs is highly correlated with cognitive impairment and functional decline[1, 2, 8, 9]. However, in previous studies with the laser-induced microhemorrhage model used here, we found that these small bleeds cause neither the death of nearby neurons nor the degeneration of their dendritic arbors[11]. We also found that while neurons near the injury initially lost their ability to respond to a stimulus, they recovered within hours[12]. We did find that microhemorrhages led to a rapidly-initiated inflammatory response, as indicated by an increased density of CX3CR1^{+} cells in the vicinity of the lesion, that was sustained for weeks[11]. In this work, we used a series of *in vivo* imaging and histological studies to follow the behavior of several different inflammatory cell types after the induction of ~100-μm sized hemorrhages in healthy adult mice. The initial inflammatory response was dominated by brain-resident microglia, which exhibited a coordinated pattern of migration and proliferation that led to an increased density of microglia near the lesion over hours to days (primarily by migration from the surrounding tissue), while later recovering the density of microglia in the surrounding tissue (by proliferation). We also found reactive astrocytes over a similar spatial region as microglia, but with the response delayed by a few days relative to microglia. The delayed astrocyte activation could be explained by the recent finding that activated, inflammatory microglia induce astrocyte activation by releasing cytokines[23]. A small number of Mo/MΦ were also identified in the brain near the lesion, with CCR2^{+} Mo/

MΦ found in the first couple of days, and CX3CR1^{+} Mo/MΦ found later, over days to weeks after the injury.

There are several mechanisms by which the inflammation we observe after a microhemorrhage could impact neural function. In healthy brain, microglia and astrocytes play an active role in remodeling synaptic circuits[24, 25]. However, in response to inflammatory stimuli, this healthy glial-mediated rewiring can be altered. For example, under ischemic stress microglia exhibited prolonged contact with synapses and were found to phagocytize synaptic components[25]. Moreover, activation of microglia and astrocytes results in the secretion of cytotoxic factors, cytokines, chemokines, growth factors, and even neurotransmitters that tune inflammatory cell function, recruit additional leukocytes, and may also be neurotoxic and interfere with neuronal function[26-29]. Infiltrated monocytes may also secrete factors that modulate learning and memory[29]. Thus, activation and redistribution of inflammatory cells near a CMB, the phagocytic activity of these cells, and the signaling factors they secrete all likely affect the behavior of nearby neurons and other cells. The accumulation of such events may contribute to the cognitive effects associated with CMBs.

In the healthy brain, microglia are intercalated throughout the entire parenchyma and are arranged in non-overlapping domains, which they surveil by extending and retracting processes[21]. Through this surveillance, microglia detect subtle changes in the microenvironment and react to a broad variety of insults, sensed with an array of surface receptors including purigenic[22] and fractalkine[30] receptors. Like other tissue-resident macrophages, microglia maintain their population locally by proliferative self-renewal[31-34], with sporadic proliferation under normal conditions and clonal expansion under prolonged and severe pathological conditions[34]. Here, through a series of *in vivo* analyses, we describe the concerted spatiotemporal response of microglial migration and proliferation in a focal injury model. We observed proliferation of microglia predominantly in regions where the density of microglia declined due to migration of other microglia toward the lesion, suggesting that microglia may sense their local density and proliferate when the density decreases. It is not clear how microglia might sense such changes in density, but it has been reported that microglial processes repel one another when they make contact[21]. Proliferation occurred primarily at a region and time relative to the CMB in which microglia had a ramified morphology, suggesting that it is the resting-state microglia, rather than the activated microglia responding to an injury, that tend to proliferate. This proliferation compensated for the decreased microglia density due to migration toward the injury. This coordinated pattern of migration and proliferation suggests a way that microglia may maintain their characteristic organization and cellular density in non-overlapping domains after a nearby focal injury. Further work needs to be done to uncover the specific molecular mechanisms underlying this coordinated pattern of migration and proliferation in microglia, as well as to follow the fate of activated microglia after the injury.

Our study elucidated the response of a subset of inflammatory cells following a femtosecond laser induced microbleed, but our work leaves some aspects of the inflammatory response unresolved. We characterized the time course of the appearance of CX3CR1^{+} and CCR2^{+} Mo/MΦ after a microhemorrhage, but we studied the response of these cells in separate reporter mice, preventing us from elucidating the role of phenotype switching in Mo/MΦ

cells. In a focal ischemic model, it has been reported that many CCR2^{+} Mo/MΦ that had invaded after the stroke later transdifferentiated to CX3CR1^{+} Mo/MΦ[20]. Our data aligns with these findings in that CCR2^{+} Mo/MΦ are the majority blood-derived cell type present early after injury and CX3CR1^{+} Mo/MΦ are more dominant at later time points. It remains unclear however, if CCR2^{+}Mo/MΦ switched to CX3CR1^{+} Mo/MΦ or if CX3CR1^{+} Mo/MΦ separately invaded. In addition, we cannot rule out the invasion of other blood borne leukocytes, although their numbers would likely be low given that the total number of labeled cells found in UBC-GFP → wild-type BMT mice approximately matched the sum of cells found in CX3CR1$^{GFP/+}$ → wild-type BMT mice and CCR2$^{RFP/+}$ mice. In addition, endogenous brain cells other than microglia and astrocytes, such as oligodendrocytes and perivascular macrophages, could have also participated in the initiation and resolution of inflammatory responses caused by laser induced microhemorrhages, all of which needs further work. Finally, our work was conducted in healthy adult animals and the cascade of inflammatory response may differ considerably in older mice[35] or in animals with co-morbidities such as CAA[36].

Conclusion

Here in this work, a single event of bleeding from a penetrating arteriole induced an inflammatory response that spanned more than a week and was characterized by microglia and later astrocyte activation as well as the presence of monocyte-derived tissue macrophages of different phenotypes. Although this small bleed does not cause direct neuronal degeneration[11] nor loss of responsiveness to external stimuli[12], this prolonged inflammatory response could cause subtle modulation of normal brain function, and the accumulation of such events could underlie cognitive decline.

Supplementary Material

Refer to Web version on PubMed Central for supplementary material.

Acknowledgments

Confocal images were acquired through the Cornell University Biotechnology Resource Center, with NYSTEM (CO29155) and NIH (S10OD018516) funding for the shared Zeiss LSM880 confocal/multiphoton microscope. We thank Sylvie Allen and Kevin Yager in the Cornell Center for Animal Resources and Education for assistance with the mouse irradiation for bone marrow transplants.

Sources of Funding: This work was supported by the National Institutes of Health grants NS080098 (C.S.), NS081179 (J.A.), and American Heart Association grant 16PRE27600010 (S.A.).

References

1. Ungvari Z, Tarantini S, Kirkpatrick AC, Csiszar A, Prodan CI. Cerebral microhemorrhages: Mechanisms, consequences, and prevention. American journal of physiology Heart and circulatory physiology. 2017; 312:H1128–h1143. [PubMed: 28314762]
2. Wiegman AF, Meier IB, Schupf N, Manly JJ, Guzman VA, Narkhede A, et al. Cerebral microbleeds in a multiethnic elderly community: Demographic and clinical correlates. J Neurol Sci. 2014; 345:125–130. [PubMed: 25091451]

3. Wakisaka Y, Chu Y, Miller JD, Rosenberg GA, Heistad DD. Spontaneous intracerebral hemorrhage during acute and chronic hypertension in mice. Journal of cerebral blood flow and metabolism. 2010; 30:56–69. [PubMed: 19724290]
4. Vinters HV, Gilbert JJ. Cerebral amyloid angiopathy: Incidence and complications in the aging brain. Ii. The distribution of amyloid vascular changes. Stroke. 1983; 14:924–928. [PubMed: 6658996]
5. Charidimou A, Shakeshaft C, Werring D. Cerebral microbleeds on magnetic resonance imaging and anticoagulant-associated intracerebral hemorrhage risk. Frontiers in neurology. 2012:3. [PubMed: 22347208]
6. Vitali P, Boghen D, Daneault N, Guillon-Letourneau L, Poppe AY. Cerebral microbleed causing an acute stroke-like episode in a cadasil patient. The Canadian journal of neurological sciences. 2014; 41:661–663. [PubMed: 25373821]
7. Charidimou A, Law R, Werring DJ. Amyloid “spells” trouble. The Lancet. 2012; 380:1620.
8. Poels MMF, Ikram MA, van der Lugt A, Hofman A, Niessen WJ, Krestin GP, et al. Cerebral microbleeds are associated with worse cognitive function the rotterdam scan study. Neurology. 2012; 78:326–333. [PubMed: 22262748]
9. Li X, Yuan J, Yang L, Qin W, Yang S, Li Y, et al. The significant effects of cerebral microbleeds on cognitive dysfunction: An updated meta-analysis. PloS one. 2017; 12:e0185145. [PubMed: 28934304]
10. Nishimura N, Schaffer CB, Friedman B, Tsai PS, Lyden PD, Kleinfeld D. Targeted insult to subsurface cortical blood vessels using ultrashort laser pulses: Three models of stroke. Nature Methods. 2006; 3:99–108. [PubMed: 16432519]
11. Rosidi NL, Zhou J, Pattanaik S, Wang P, Jin W, Brophy M, et al. Cortical microhemorrhages cause local inflammation but do not trigger widespread dendrite degeneration. PloS one. 2011; 6:e26612. [PubMed: 22028924]
12. Cianchetti FA, Kim DH, Dimiduk S, Nishimura N, Schaffer CB. Stimulus-evoked calcium transients in somatosensory cortex are temporarily inhibited by a nearby microhemorrhage. PloS one. 2013:8.
13. Schrag M, McAuley G, Pomakian J, Jiffry A, Tung S, Mueller C, et al. Correlation of hypointensities in susceptibility-weighted images to tissue histology in dementia patients with cerebral amyloid angiopathy: A postmortem mri study. Acta Neuropathologica. 2010; 119:291–302. [PubMed: 19937043]
14. Dichgans M, Holtmannspotter M, Herzog J, Peters N, Bergmann M, Yousry TA. Cerebral microbleeds in cadasil: A gradient-echo magnetic resonance imaging and autopsy study. Stroke. 2002; 33:67–71. [PubMed: 11779891]
15. Fazekas F, Kleinert R, Roob G, Kleinert G, Kapeller P, Schmidt R, et al. Histopathologic analysis of foci of signal loss on gradient-echo t2*-weighted mr images in patients with spontaneous intracerebral hemorrhage: Evidence of microangiopathy-related microbleeds. *AJNR.* American journal of neuroradiology. 1999; 20:637–642. [PubMed: 10319975]
16. Fisher M, French S, Ji P, Kim RC. Cerebral microbleeds in the elderly: A pathological analysis. Stroke. 2010; 41:2782–2785. [PubMed: 21030702]
17. Jin R, Yang G, Li G. Inflammatory mechanisms in ischemic stroke: Role of inflammatory cells. Journal of leukocyte biology. 2010; 87:779–789. [PubMed: 20130219]
18. Gelderblom M, Leypoldt F, Steinbach K, Behrens D, Choe CU, Siler DA, et al. Temporal and spatial dynamics of cerebral immune cell accumulation in stroke. Stroke. 2009; 40:1849–1857. [PubMed: 19265055]
19. Benakis C, Garcia-Bonilla L, Iadecola C, Anrather J. The role of microglia and myeloid immune cells in acute cerebral ischemia. Front Cell Neurosci. 2014; 8:461. [PubMed: 25642168]
20. Garcia-Bonilla L, Faraco G, Moore J, Murphy M, Racchumi G, Srinivasan J, et al. Spatio-temporal profile, phenotypic diversity, and fate of recruited monocytes into the post-ischemic brain. Journal of neuroinflammation. 2016; 13:285. [PubMed: 27814740]
21. Nimmerjahn A, Kirchhoff F, Helmchen F. Resting microglial cells are highly dynamic surveillants of brain parenchyma in vivo. Science. 2005; 308:1314–1318. [PubMed: 15831717]

22. Davalos D, Grutzendler J, Yang G, Kim JV, Zuo Y, Jung S, et al. Atp mediates rapid microglial response to local brain injury in vivo. Nat Neurosci. 2005; 8:752–758. [PubMed: 15895084]
23. Liddelow SA, Guttenplan KA, Clarke LE, Bennett FC, Bohlen CJ, Schirmer L, et al. Neurotoxic reactive astrocytes are induced by activated microglia. Nature. 2017; 541:481–487. [PubMed: 28099414]
24. Chung WS, Clarke LE, Wang GX, Stafford BK, Sher A, Chakraborty C, et al. Astrocytes mediate synapse elimination through megf10 and mertk pathways. Nature. 2013; 504:394–400. [PubMed: 24270812]
25. Wake H, Moorhouse AJ, Jinno S, Kohsaka S, Nabekura J. Resting microglia directly monitor the functional state of synapses in vivo and determine the fate of ischemic terminals. Journal of Neuroscience. 2009; 29:3974–3980. [PubMed: 19339593]
26. Schneider H, Pitossi F, Balschun D, Wagner A, del Rey A, Besedovsky HO. A neuromodulatory role of interleukin-1beta in the hippocampus. Proceedings of the National Academy of Sciences of the United States of America. 1998; 95:7778–7783. [PubMed: 9636227]
27. Tancredi V, D'Antuono M, Cafè C, Giovedì S, Buè MC, D'Arcangelo G, et al. The inhibitory effects of interleukin-6 on synaptic plasticity in the rat hippocampus are associated with an inhibition of mitogen-activated protein kinase erk. Journal of Neurochemistry. 2000; 75:634–643. [PubMed: 10899938]
28. Beattie EC, Stellwagen D, Morishita W, Bresnahan JC, Ha BK, Von Zastrow M, et al. Control of synaptic strength by glial tnfalpha. Science. 2002; 295:2282–2285. [PubMed: 11910117]
29. Donzis EJ, Tronson NC. Modulation of learning and memory by cytokines: Signaling mechanisms and long term consequences. Neurobiology of learning and memory. 2014; 115:68–77. [PubMed: 25151944]
30. Fuhrmann M, Bittner T, Jung CK, Burgold S, Page RM, Mitteregger G, et al. Microglial cx3cr1 knockout prevents neuron loss in a mouse model of alzheimer's disease. Nat Neurosci. 2010; 13:411–413. [PubMed: 20305648]
31. Mildner A, Schmidt H, Nitsche M, Merkler D, Hanisch UK, Mack M, et al. Microglia in the adult brain arise from ly-6chiccr2+ monocytes only under defined host conditions. Nat Neurosci. 2007; 10:1544–1553. [PubMed: 18026096]
32. Ajami B, Bennett JL, Krieger C, Tetzlaff W, Rossi FM. Local self-renewal can sustain cns microglia maintenance and function throughout adult life. Nat Neurosci. 2007; 10:1538–1543. [PubMed: 18026097]
33. Askew K, Li K, Olmos-Alonso A, Garcia-Moreno F, Liang Y, Richardson P, et al. Coupled proliferation and apoptosis maintain the rapid turnover of microglia in the adult brain. Cell reports. 2017; 18:391–405. [PubMed: 28076784]
34. Tay TL, Mai D, Dautzenberg J, Fernandez-Klett F, Lin G, Sagar, et al. A new fate mapping system reveals context-dependent random or clonal expansion of microglia. Nat Neurosci. 2017; 20:793–803. [PubMed: 28414331]
35. Sumbria RK, Grigoryan MM, Vasilevko V, Paganini-Hill A, Kilday K, Kim R, et al. Aging exacerbates development of cerebral microbleeds in a mouse model. Journal of neuroinflammation. 2018; 15:69. [PubMed: 29510725]
36. Marinescu M, Sun L, Fatar M, Neubauer A, Schad L, van Ryn J, et al. Cerebral microbleeds in murine amyloid angiopathy. Stroke. 2017; 48:2248–2254. [PubMed: 28706123]

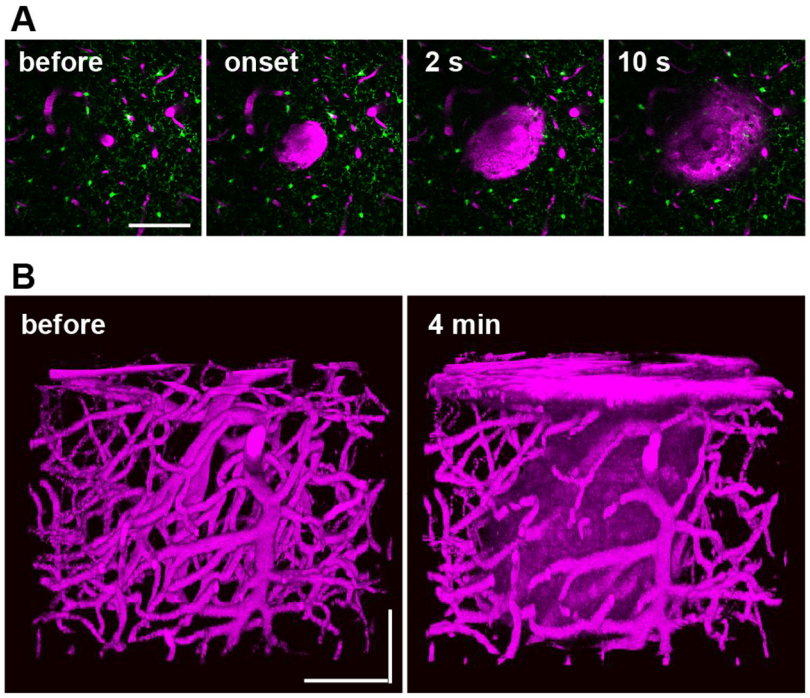

Figure 1. Femtosecond laser-induced cortical microhemorrhages

(**A**) In vivo two-photon excited fluorescence images of fluorescently-labeled blood plasma (magenta, i.v. injected Texas Red dextran) during creation of a microhemorrhage by ablation of a cortical penetrating arteriole. (**B**) 3D reconstruction of the vasculature and extravagated plasma before and after the lesion. All scale bars are 100 μm.

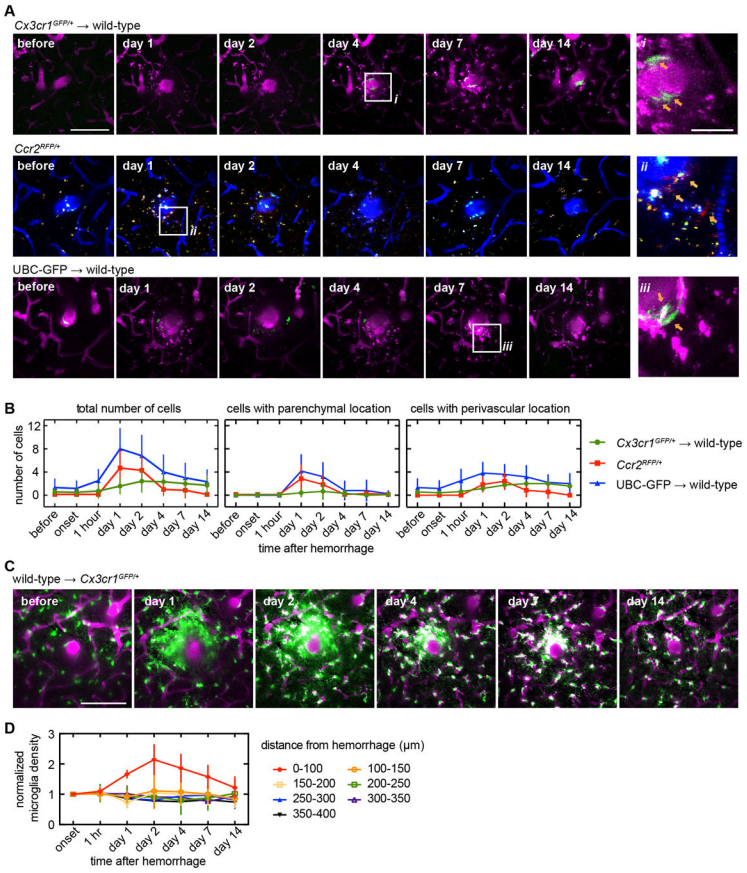

Figure 2. Invasion of a small number of blood-borne inflammatory cells and an increase in density of brain-resident microglia were observed over a few days near the microhemorrhage

(**A**) Axial projections of two-photon image stacks showing the response of different genetically-labeled inflammatory cell types over 2 weeks after a microhemorrhage. In wild-type animals receiving a *Cx3cr1*$^{GFP/+}$ bone marrow transplant (*Cx3cr1*$^{GFP/+}$ → wild-type), labeled cells are patrolling monocytes (top panel, green, GFP). In *CCR2*$^{RFP/+}$ animals, labeled cells are inflammatory monocytes (middle panel, red, RFP; blue, i.v. injected Cascade Blue dextran). In UBC-GFP → wild-type animals, all types of circulating cells other than red blood cells are labeled (bottom panel, green, GFP). Location of insets (on right) are indicated with white boxes. (**B**) Number of cells within the image volume (230 × 230 × 40 μm, centered on microhemorrhage) over time for the same genetically-labeled cell populations show in A (left). The same data was broken down by cell location perivascular (defined as the cell touching the outside of the vessel; middle) and parenchymal (right) locations. (*Cx3cr1*$^{GFP/+}$ → wild-type: n=12 in 4; *CCR2*$^{RFP/+}$: n=6 in 3; UBC → wild-type: n=7 in 2). (**C**) In *Cx3cr1*$^{GFP/+}$ animals receiving a wild-type bone marrow transplant (wild-type → *Cx3cr1*$^{GFP/+}$), labeled cells are nearly all microglia (green, GFP). Axial projections (40 μm thick) of two-photon image stacks showing the response of microglia over 2 weeks after a microhemorrhage (magenta, i.v. injected Texas Red dextran; green, GFP). (**D**) Plot of normalized density of microglia over time after a microhemorrhage for regions at different distance from the lesion (wild-type → *Cx3cr1*$^{GFP/+}$: n=5 hemorrhages from 3 mice). All scale bars are 100 μm, except for the insets in (A), which are 25 μm. Error bars indicate SD.

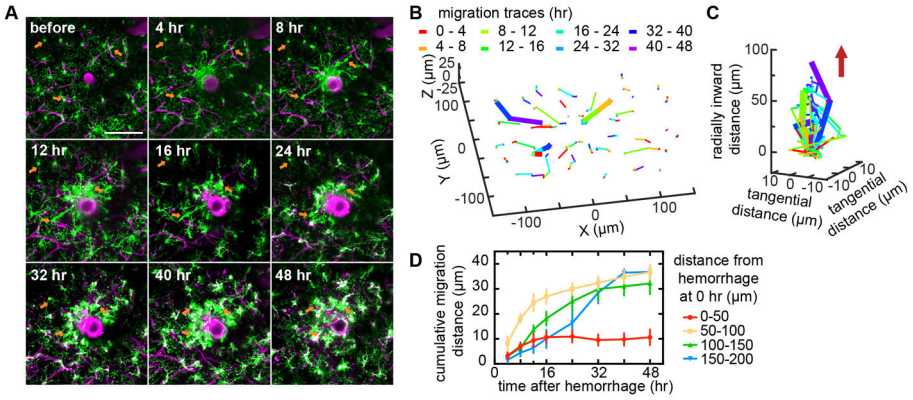

Figure 3. Local increase in microglia density was due to migration of nearby microglia toward the injury

(**A**) Axial projections of 40-μm thick two photon image stacks over time after a microhemorrhage in a *Cx3cr1*$^{GFP/+}$ mouse. (**B**) Migration paths of the microglia from panel (A). The color of the segment indicates the time span when that migration occurred. The three bold paths correspond to the three cells identified with orange arrows in (A). (**C**) Data from (B) plotted with the radial migration toward the lesion from the initial location of each microglia on the z-axis. The red arrow indicates the direction of the microhemorrhage. The color of the segment in (B) and (C) indicates the time span when that migration occurred. (**D**) Cumulative radial migration distance toward the microhemorrhage for microglia with different initial distances from the target vessel (n=4 hemorrhages from 3 mice). All scale bars are 100 μm. Error bars indicate SD.

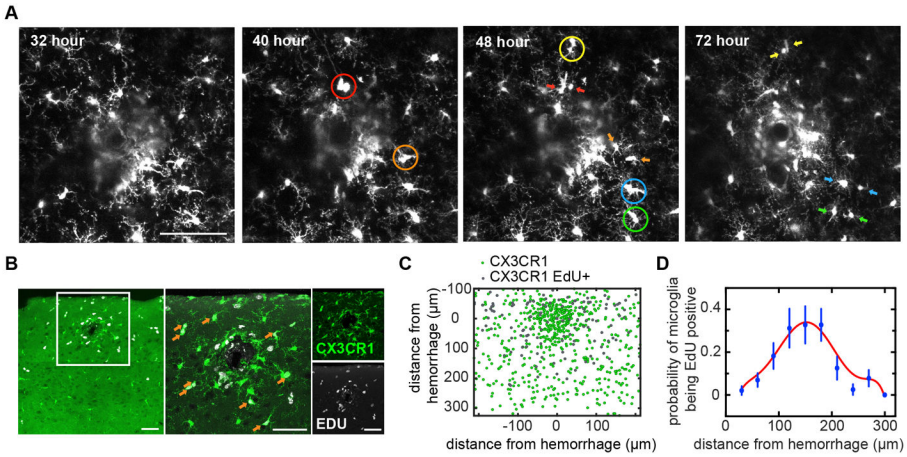

Figure 4. Proliferation of microglia was observed in a shell-shaped region surrounding the lesion

(**A**) Axial projections of 40-μm thick 2PEF image stacks over time after a microhemorrhage in a *Cx3cr1*$^{GFP/+}$ mouse. Colored circles indicate cells that will proliferate by the next time point. Arrows with matching colors indicate the pair of daughter cells. Scale bar is 100 μm. The full time series of this particular hemorrhage is shown in Supplementary fig. IIA. (**B**) Images of a coronal histological section that intersected a microhemorrhage from an animal sacrificed two days after the lesion and with repeated EdU injections. Cells that proliferated over those two days are labeled with EdU (white), while microglia are labeled with GFP (green). The white box in the left image indicates the region for the magnified images to the right. (**C**) Composite map of the location of all microglia and EdU+ microglia from coronal sections across 17 hemorrhages from three mice, with the location of the microhemorrhage centers aligned at (0,0). The cortical surface is at the top of the image. (**D**) The probability of microglia being EDU positive as a function of radial distance from the microhemorrhage from the data shown in (C) and a polynomial fit (red trend line). All scale bars are 100 μm.

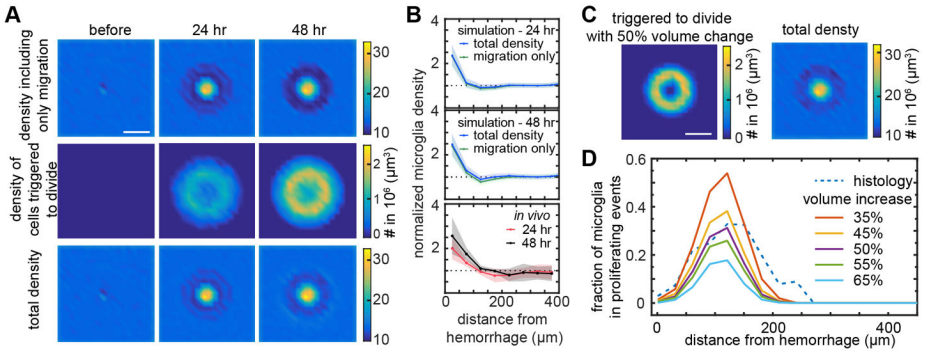

Figure 5. Simulation of microglia density changes due to migration and proliferation after a microhemorrhage

(**A**) Map of the density of microglia including only migration and not proliferation in the simulation (top), of microglia committed to division (middle), and of total microglia density (bottom) at baseline and at 24 and 48 hrs after the microhemorrhage. (**B**) Plot of normalized density of microglia as a function of distance from a microhemorrhage at 24 (top) and 48 (middle) hrs after the injury for the simulation showing the density including migration and proliferation (blue) or just migration (green). The lower plot shows experimental *in vivo* measurements at 24 (red) and 48 (black) hrs after the lesion (same data as shown in Fig. 3B; n=5 hemorrhages from 3 mice). Lines (shading) indicate mean (SD). (**C**) Map of the total density of microglia (left) and of the density of microglia committed to division (right) at 48 hrs after a microhemorrhage using models where microglia proliferation occurs when the domain volume of a microglia increases by more than 50% percentage. (**D**) The fraction of microglia that have either committed to divide or are daughter cells of a proliferation event as a function of distance from and at 48 hrs after the microhemorrhage for different density-dependent microglia proliferation models. The dashed line represents the fraction of microglia that were found to be EdU positive in experiments (same data as in Fig. 4D). Scale bars are 200 μm.

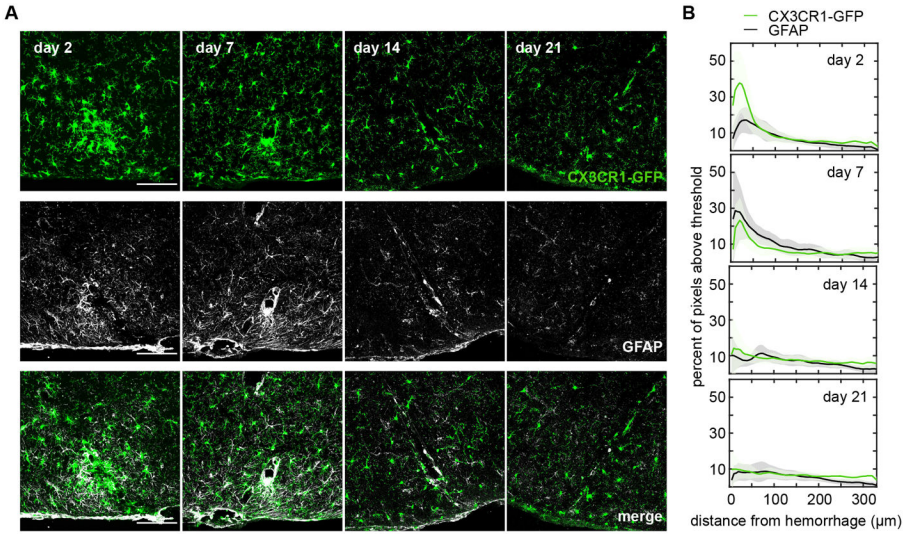

Figure 6. Astrocyte activation was observed in the region of microglia density increase, but peaked at later times

(**A**) Images of coronal histological section that intersected a microhemorrhage from animals sacrificed 2, 7, 12, and 21 days after the lesion. Microglia were visualized by the expression of CX3CR1-GFP (top panels), astrocytes were visualized by immunolabeling of GFAP (middle panels). The bottom panels show an overlay. Cortical surface is to the bottom of the images. (**B**) The percent of image pixels above a threshold as a function of distance away from the lesion and over time for microglia and astrocytes. Data represents the average of 6-9 hemorrhages across 2-3 mice for each time point. Scale bars are 100 μm.